ACS OMEGA

http://pubs.acs.org/journal/acsodf

Article

Water-Soluble Pyrene-Adorned Imidazolium Salts with Multicolor Solid-State Fluorescence: Synthesis, Structure, Photophysical Properties, and Application on the Detection of Latent Fingerprints

Muthukumaran Nirmala, Ramanan Vadivel, Selvaraju Chellappan, Jan Grzegorz Malecki, and Perumal Ramamurthy*

Cite This: *ACS Omega* 2021, 6, 10318−10332

Read Online

ACCESS | Metrics & More | Article Recommendations | Supporting Information

ABSTRACT: New water-soluble acetylpyrene-bound imidazolium salts (1-*N*-methyl-3-(2-oxo-2-(pyren-1-yl)ethyl)-imidazolium bromide (**1**), 1-*N*-isopropyl-3-(2-oxo-2-(pyren-1-yl)ethyl)-imidazolium bromide (**2**), 1-*N*-allyl-3-(2-oxo-2-(pyren-1-yl)ethyl)-imidazolium bromide (**3**), and 1-*N*-isopropyl-3-(2-oxo-2-(pyren-1-yl)ethyl)-imidazolium hexafluorophosphate (**4**)) were synthesized from the reaction between 1-bromoacetylpyrene and N-substituted imidazoles in excellent yield. The new molecules were fully characterized by elemental analysis, FT-IR, multinuclear (^{1}H, ^{13}C, and ^{19}F) NMR techniques, and single-crystal X-ray diffraction analysis. Investigations on the crystal packing of **1**, **3**, and **4** show the presence of inter/intramolecular weak interactions, including the $\pi\cdots\pi$ stacking interaction between the pairs of pyrene molecules. The photophysical properties were investigated in detail for the four imidazolium salts. Experiments show that the emissions observed for all the four compounds are due to the excited monomer and static excimer. Very interestingly, all the four compounds exhibit solid-state multicolor fluorescence depending on the excitation wavelength. The solid-state emissions were monitored using a fluorescence microscope. Finally, a fingerprint powder was formulated based on compound **4** and demonstrated as an efficient fluorescent fingerprint powder for forensic applications. The formulated powder revealed all the 3 level information along with peculiar individual characteristics of the fingerprints under investigation. The fingerprints were further viewed through a fluorescence microscope, and the results were discussed in detail.

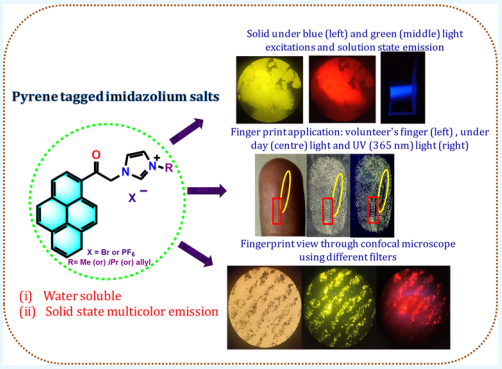

1. INTRODUCTION

Although known for many decades, it is only in the past ten years that *N*-heterocyclic carbenes (NHCs) were undoubtedly positioned in the front rows of the molecular matrix and play a prominent role in chemistry with consecutively emerging applications in organic, organometallic, and main-group elements chemistry.[1] Despite the rapid evolution, the applications of NHCs are relatively scarce in fields other than catalysis.[2] In recent years, the NHCs have received significant attention in the field of surface chemistry, luminescent materials, gas absorption and separation, dye-sensitized solar cells, medicine, and sensors.[3−11] 2*H*-Imidazole-2-ylidenes are the most classical compound of this class of NHCs.[12−14] The classical NHCs are five-membered-ring compounds, in which the carbene donor is located adjacent to two nitrogen atoms.[15,16] The substituents at these α-nitrogen atoms can be altered to tune the stereo-electronic properties of the NHC molecule.[17] The great structural versatility and unprecedented behavior of NHCs allow the design of multiple architectures with interesting chemical and electro−optical properties.[18] Currently, fluorescent-tagged NHCs have asserted significant attention due to their promising applications in sensors and organic electronic applications.[19,20] Moreover, presence of an organic chromophore on imidazolium nitrogen is usually required to impart the desired fluorescence property of imidazolium salt.[21−26] As a result, the fascinating characteristics of fluorophores can be combined with the typical properties of imidazolium salts. This cooperation has been tuned to increase the efficiency of the resulting salts in the finding of new optical devices on various fields.

Since the invention of luminescent organic devices[27] in 1995, there has been increasing interest in designing novel materials with very good emissive properties due to their fascinating applications in fields such as optoelectronic devices, data storage, memory devices, fluorescent probe for bio applications, and thin-film transistors.[28−32] Indeed, organic emitters have

Received: February 5, 2021
Accepted: March 19, 2021
Published: April 9, 2021

Scheme 1. Synthesis of Acetylpyrene Imidazolium NHC Ligands (1−4)

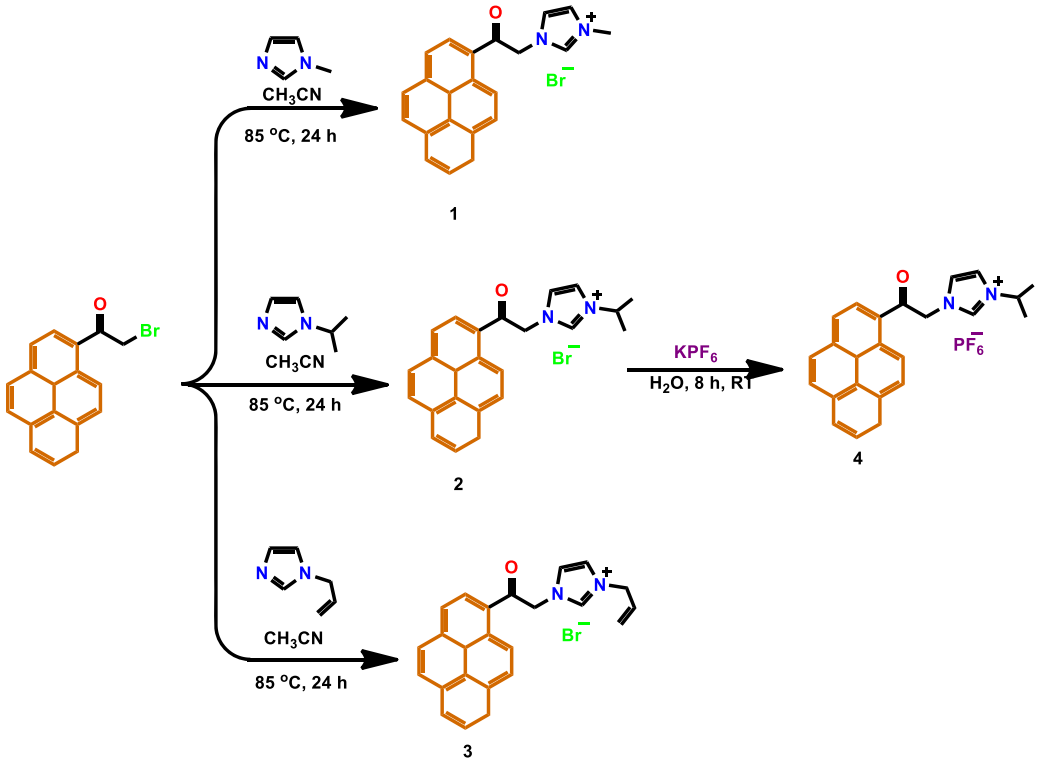

several advantages compared to inorganic emitters, including high brightness, good photostability, quantum efficiency, large Stokes shift, and biocompatibility.[33−35] Nonetheless, the design and synthesis of light-emitting compounds with suitable multifunctional properties for high-performance OLEDs (organic light emitting diodes) remain a challenge. Based on recent investigations, pyrene and its derivatives are the most studied organic chromophores[30] and are found to have widespread applications in photonic devices.[36,37] Pyrene possesses an exceptionally longer fluorescence lifetime and polarity-sensitive vibronic emission, high charge carrier mobility, $\pi-\pi$ stacking behavior, and chemical stability.[35,38] However, there are two major disadvantages that limit the use of pyrene in organic luminescent materials. At first, the excimer formation observed in condensed solution and solid state leads to a dramatic decline in fluorescence intensity.[39] Second, the absorption and emission regions of pyrene fluorophores lie in the near UV region, whereas most optoelectronic applications engrossed the emission in the visible region.[40] Consequently, the purpose of this study was to explore the lucid design of pyrene derivatives with suitable substituents that exhibit intense visible region emission in the solid state. Based on the above facts, various substituted (methyl, *i*Pr, and allyl) imidazoles, tagged with fluorescent, conjugated pyrene moieties (**1**−**4**) were designed and synthesized in this work. Both the NHC and the conjugated pyrene skeleton can be tuned by extending their π-conjugation to shift their absorption and emission bands to the visible region of the electromagnetic spectrum. We have briefly studied the photophysical properties of the pyrene-tagged NHC derivatives in aqueous or semi-aqueous media as well as in the solid state. Interestingly, all the derivatives in this study exhibit solid-state fluorescence. Depending on the excitation wavelength, they show yellow and red color emissions in the solid state which extends the applications of these compounds in various fields such as OLED, sensors, phosphors, and so forth.[41,42] Moreover, the red emissive nature of these compounds makes them as a possible candidate for bioimaging applications. In this study, we have exploited the solid-state fluorescence behavior of the pyrene-tagged NHC derivatives toward the detection of latent fingerprints in forensic investigations and presented our preliminary results. Fluorescent fingerprint powders find their applications in the decipherment of latent fingerprints deposited on multicolored surfaces where the commercial powders fail due to lack of contrast between the powder and the background. Apart from that the longer wavelength emission of the compounds reported here allows a forensic fingerprint examiner to develop the latent fingerprints on multicolored, emissive surfaces such as currency notes, papers, plastics, and so forth which are challenging surfaces in forensic investigations.[43]

2. RESULTS AND DISCUSSION

2.1. Synthesis and Characterization. The *N*-methyl substituted imidazolium salt (**1**) was obtained according to the known literature procedure.[44] The syntheses of *N*-isopropyl (**2**) and *N*-allyl (**3**)-substituted imidazolium salts were performed by the direct alkylation of 1-(bromoacetyl)pyrene with a variety of *N*-substituted imidazoles [Me (**1**), iPr (**2**), and allyl (**3**)] in acetonitrile at 85 °C for 24 h under a N_2 atmosphere. The synthetic strategy is shown in Scheme 1. After purification, the acetylpyrene imidazolium salts **1**, **2**, and **3** were obtained in excellent yield. Anion metathesis reaction of **2** with KPF_6 was carried out at room temperature in the aqueous medium, which furnished the corresponding hexafluorophosphate salt **4** in 82% yield. The salts **1**, **2**, and **3** were highly soluble in water, whereas salt **4** was highly soluble in acetone, acetonitrile, methanol, DMF and DMSO, and so forth and almost insoluble in hexane and diethyl ether. The new salts **1**−**4** were fully characterized by elemental analysis, FT-IR, multinuclear NMR (^{1}H, ^{13}C, and ^{19}F)

https://doi.org/10.1021/acsomega.1c00679
ACS Omega 2021, 6, 10318−10332

Table 1. Crystal Data and Structure Refinement Parameters for Acetylpyrene Imidazolium Salts (1, 3, and 4)

	1	3	4
CCDC number	1,986,848	1,986,849	1,986,847
empirical formula	$C_{22}H_{19}N_2O_2Br_1$	$C_{24}H_{19}N_2O_1Br_1$	$C_{24}H_{21}N_2O_1F_6P_1$
formula weight	423.30	431.32	498.40
T (K)	295(2)	295(2)	295(2)
wavelength (Å)	0.71073	0.71073	0.71073
crystal system	Monoclinic	orthorhombic	monoclinic
space group	$P2_1/c$	*Pbcn*	$P2_1/c$
unit cell dimensions			
a (Å)	16.3680(14)	12.7276(6)	15.0326(17)
b (Å)	8.0391(5)	10.6077(5)	19.4866(7)
c (Å)	14.6569(9)	28.7845(13)	7.4531(3)
α (°)	90.00	90.00	90.00
β (°)	99.062(7)	90.00	99.450(4)
γ(°)	90.00	90.00	90.00
volume (Å^3)	1904.5 (2)	3886.2(3)	2183.19 (16)
Z	4	8	4
density (calculated) Mg m^{-3}	1.476	1.474	1.516
absorption coefficient mm^{-1}	2.178	2.133	0.198
F(000)	864	1760	1024
scan range for data collection (deg)	3.831 to 25.638	4.0920 to 25.7500	4.1370 to 27.9060
index ranges	$-21 <= h = 22$, $-10 <= k = 8$, $-19 <= l = 19$	$-17 <= h = 10$, $-12 <= k = 13$, $-29 <= l = 39$	$-20 <= h = 13$, $-26 <= k = 26$, $-9 <= l = 10$
reflections collected/unique, R_{int}	14391/4653, 0.0570	14864/4722, 0.0470	17422/5328, 0.0574
completeness to theta$_{max}$	0.995	0.886	0.997
data/restraints/parameters	4653/0/253	4772/0/253	5328/0/309
goodness-of-fit on F^2	1.004	1.021	1.019
final *R* indices [$I > 2\sigma(I)$][a]	$R_1 = 0.0570$, $wR_2 = 0.1047$	$R_1 = 0.0470$, $wR_2 = 0.0911$	$R_1 = 0.0574$, $wR_2 = 0.1366$
R indices (all data)	$R_1 = 0.1403$, $wR_2 = 0.1317$	$R_1 = 0.0944$, $wR_2 = 0.1066$	$R_1 = 0.1106$, $wR_2 = 0.1601$

[a]Structures were refined on F_o^2: $wR_2 = [\sum[w(F_o^2 - F_c^2)^2]/\sum w(F_o^2)^2]^{1/2}$, where $w^{-1} = [\sum(F_o^2) + (aP)^2 + bP]$ and $P = [\max(F_o^2,0) + 2F_c^2]/3$.

analysis, and single-crystal X-ray diffraction analysis (**1**, **3**, and **4**).

In FT-IR analysis, acetylpyrene imidazolium salts **1**−**4** (Figure S1, Supporting Information) showed an intense band for ν(C═O) stretching vibrations around 1681−1678 cm^{-1}. The ν(C═N) stretching peaks were observed around 1595−1591 cm^{-1}. The formation of **1**−**4** was further evident from NMR spectroscopy. The ^{1}H NMR spectrum of imidazolium salts **1**−**4** (Figures S2−S5, Supporting Information) displayed a single resonance peak for carbenic protons at 9.27, 9.42, 9.32, and 9.33 ppm. The aromatic protons appeared in the region of 9.07−8.19 ppm. The CH$_{imidazole}$ protons appeared in the region of 8.33−7.89 ppm. The singlet corresponding to the −CH$_3$ proton(s) appeared at 4.04 ppm. The salts **2** and **4** showed a doublet in the region 1.59−1.57 ppm, which is attributed to methyl protons. Compound **3** showed a multiplet in the region 6.20−6.13 ppm for CH═CH$_2$. Besides, **3** showed a doublet in the region 5.46−5.43 ppm for CH═CHH*trans*, and a doublet appeared around 5.43−5.36 ppm which is due to CH═CHH*cis*. The NCH$_2$ proton exhibits a singlet at 6.36, 6.32, 6.35, and 6.26 ppm for NCH$_2$ protons in acetylpyrene imidazolium salts **1**−**4**. In the ^{13}C NMR spectrum (Figure S6−S9, Supporting Information), the carbenic carbon resonates at 138.38, 136.76, 136.74, and 138.08 ppm, respectively. The C═O resonates at 194.60, 194.55, 194.55, and 194.48 ppm. The peak that appeared between 134.96 and 124.51 ppm was attributed to the aromatic carbons. A signal for the CH$_3$ carbon appeared at 36.53 ppm. The characteristic signal around 123.81−120.69 ppm is due to imidazole backbone carbons C3 and C4. The CH═CH$_2$ carbon resonates at 130.74 ppm. Also, CH═CH$_2$ carbon was observed at 122.74 ppm. The signal that appeared at 51.5 ppm is assigned to CH$_2$ carbon. The presence of a PF6$^-$counter anion was confirmed by ^{19}F nuclear magnetic resonance spectroscopy (Figure S10, Supporting Information) where two singlets appeared at −62.21 and −74.76 ppm. This confirms the presence of PF6$^-$as a counter anion in acetylpyrene imidazolium salt **4**.[45,46]

2.2. X-Ray Crystal Structure Description of Acetyl Pyrene Imidazolium Salts 1, 3, and 4. The molecular structures of the acetyl pyrene imidazolium salts **1**, **3**, and **4** were firmly established by single-crystal diffraction analysis. The crystal data and structure refinement parameters are summarized in Table 1, and the selected bond lengths and bond angles are depicted in Table 2. The ORTEP views of the imidazolium salts **1**, **3**, and **4** are portrayed in Figures 1−3.

Suitable single crystals of salt **1** were grown by the slow evaporation of the concentrated solution of **1** in the methanol/acetone (1:1) mixture. The solid-state structure of **1** is shown in Figure 1. It crystallizes in a monoclinic crystal system with the $P2_1/c$ space group, respectively, and their asymmetric units constitute the whole molecule together with the water molecule and bromide ion. The crystal packing of **1** is different from that of the other two salts **3** and **4**. The molecule consists of a planar pyrene unit featuring a methyl imidazolium unit in an obtuse angle (111.0(3)) orientation. The crystal packing properties of salt **1** were highly influenced by the π-stacking interaction between pairs of molecules, and it is shown in Figure 1. Each dimer is assembled in a head-to-tail π-stacked dimer fashion. The distance of the pyrene−pyrene $\pi\cdots\pi$ stacking interaction is 3.389 Å (distance between ring centroids 1.42 Å). The bond

https://doi.org/10.1021/acsomega.1c00679
ACS Omega 2021, 6, 10318−10332

Table 2. Selected Geometrical Parameters for Complexes 1, 3, and 4

	1	3	4
Interatomic Distances (Å)			
O(1)−C(5)	1.210(4)	1.207(3)	1.216(3)
N(1)−C(1)	1.313(4)	1.321(3)	1.321(3)
N(1)−C(3)	1.353(5)	1.371(3)	1.356(3)
N(1)−C(4)	1.454(4)	1.457(3)	1.453(3)
N(2)−C(1)	1.314(4)	1.324(3)	1.315(3)
N(2)−C(2)	1.361(5)	1.370(3)	1.371(4)
N(2)−C(22)	1.476(4)	1.469(3)	1.484(4)
C(1)−H(1)	0.9300	0.9300	0.9300
C(4)−C(5)	1.524(5)	1.514(4)	1.517(3)
C(5)−C(6)	1.478(4)	1.488(3)	1.472(3)
C(22)−C(23)		1.484(6)	1.464(5)
C(22)−C(24)		1.226(6)	1.488(5)
P(1)−F(1)			1.5799(16)
P(1)−F(2)			1.5968(16)
P(1)−F(3)			1.582(2)
P(1)−F(4)			1.5694(19)
P(1)−F(5)			1.575(2)
P(1)−F(6)			1.5671(19)
Bond Angles (°)			
C(1)−N(1)−C(3)	108.2(3)	108.4(2)	107.8(2)
C(1)−N(1)−C(4)	127.0(3)	126.0(2)	125.26(19)
C(3)−N(1)−C(4)	124.6(3)	125.5(2)	126.9(2)
C(1)−N(2)−C(2)	107.7(3)	108.5(2)	107.1(2)
C(1)−N(2)−C(22)	125.6(4)	126.2(2)	127.5(2)
C(2)−N(2)−C(22)	126.6(4)	125.2(2)	124.8(2)
N(1)−C(1)−N(2)	109.0(3)	108.5(2)	109.7(2)
N(1)−C(1)−H(1)	125.5	125.7	125.1
N(2)−C(1)−H(1)	125.5	125.7	125.1
N(1)−C(4)−C(5)	111.0(3)	112.9(2)	112.80(19)
O(1)−C(5)−C(4)	116.8(3)	119.5(2)	117.9(2)
O(1)−C(5)−C(6)	125.5(3)	124.6(2)	125.1(2)
C(6)−C(5)−C(4)	117.6(3)	115.8(2)	116.99(19)
C(24)−C(23)−C(22)		130.5(4)	114.3(4)

distance between the adjacent nitrogen atoms and the center carbene carbon is in the range of N(1)−C(1)−1.313(4) Å, and the dihedral angle of N(1)−C(1)−N(2) is 109.0(3)°, which is close to the value of other imidazolium salts **4** [N(1)−C(1)−N(2), 109.7(2)°] and **3** [N(1)−C(1)−N(2), 108.5(2)°]. Furthermore, the interatomic distance of C(5)−O(1) is comparable with all the three salts [**1**, 1.210(4) Å; **3**, 1.207(3) Å; **4**, 1.216(3) Å]. Notably, the space-filling model of **1** confirms the presence of bulky planar pyrene rings attached little far away from the imidazolium ring, which in principle should allow the molecule to acclimate itself to the incoming metal without much hindrance. Salt **1** was stabilized by the weak intermolecular electrostatic interaction between the respective anion, acetylpyrene imidazolium moiety, and the water molecule. The strength of these electronic interactions and the steric size of the anions describe the differences in crystal packing. The intermolecular distances ranging for C−H···Br and C−H···O contacts are 2.751 and 2.486 Å.

Single crystals of high enough quality for X-ray diffraction analysis were obtained by the slow evaporation of concentrated acetonitrile solution of **3** at room temperature. **3** crystallizes in the orthorhombic crystal system with the *P*bcn space group, and eight molecular units are residing at one unit cell. The crystallographic data for salt **3** is collated in Tables 1 and 2, and the solid-state structure is reported in Figure 2. The asymmetric unit of **3** contains the acetyl pyrene moiety attached to the imidazole-bearing allyl arm. The geometrical orientation of 1-*N*-allyl-3-(2-oxo-2-(pyren-1-yl)ethyl)-imidazolium core of **3** is comparable to that of 1-*N*-isopropyl-3-(2-oxo-2-(pyren-1-yl)ethyl)-imidazolium core **4**. The allyl imidazolium ring is not coplanar with the central pyrene ring but has the torsion angle of 75.9(4)° [C(1)−(N(1)−C(4)−C(5)] and 8.3(4)° [C(4)−C(5)−C(6)−C(7)]. The interplanar distance between the two adjacent pyrene moieties is 5.554 Å, and the parameters are not in the range for establishing a $\pi\cdots\pi$ interaction between two pyrene moieties. The free twisting motion of the methylene motif is restricted by intermolecular hydrogen bonding with a nearby molecular unit. The intermolecular bond distances of C(19)−H(4A), C(18)−H(4A), H(8)−C(15), and H(8)−C(16) are 2.876, 2.881, 2.791, and 2.876 Å, respectively, suggesting the existence of the C−H···π interaction. Apart from that the intermolecular bond distances of C(4)−H(4B)···Br(1), C(3)−H(3)···Br(1), C(2)−H(2)···Br(1), C(3)−H(3)···Br(1), and C(22)−H(22B)···Br(1) are 2.649, 2.992, 2.803, 2.982, and 2.823 Å, respectively (Figure 2). Furthermore, the angle of olefin located on the imidazole ring [C(24)−C(23)−C(22)] is 130.5(4) Å, and the torsion angles between the imidazole [C(1)−(N(1)−C(4)−C(5)] and acetyl pyrene motif [C(4)−C(5)−C(6)−C(7)] are −108.2(3) and −19.5(3)°, respectively.

Single crystals suitable for X-ray diffraction analysis were obtained from an acetonitrile solution of **4** at room temperature. **4** crystallizes in the monoclinic crystal system with the $P2_1/c$ space group and four molecular units residing at the unit cell. The molecular structure, space-filling model, and side ORTEP view of **4** are portrayed in Figure 3. The asymmetric unit of **4** encapsulated with acetylpyrene is attached to the isopropyl imidazolium moiety and one $PF6^-$ counter ion. The methylene group connects the acetyl pyrene with imidazole. The pyrene ring remains planar in the structure. As shown in Figure 3, the imidazolium ring was not oriented in the same plane as pyrene. The unit cell of **3** contains two groups of differently oriented dimers. Each dimer is composed of two parallel head-to-head π-stacked pyrene groups. The $PF6^-$ moieties are trapped by organic fragments through weak inter and intramolecular C−H···F hydrogen bonds [H(10)−F(6), 2.594 Å; H(4B)−F(3), 2.401 Å]. The crystal packing of the molecule reveals the $\pi\cdots\pi$ stacking interaction between the pyrene groups of adjacent molecules. The interplanar distance for the dimer is 3.299 Å (distance between ring centroids 1.215 Å). In the acetyl pyrene unit, the bond lengths of O(1)−C(5) and C(5)−C(6) are 1.216(3) and 1.472(3) Å, respectively. Furthermore, the bond length of the methylene carbon attached to the imidazole ring is 1.455(3) Å (N(1)−C(4)). The C(1)−N(1)−C(4)−C(5) and C(4)−C(5)−C(6)−C(7) torsion angles of −101.7(3) and −24.9(3)° clearly show the non-planarity of imidazole and acetyl pyrene motifs. In addition, the intermolecular hydrogen bond distances of O(1)···H(1), C(10)−H(10)···F(6), and H(4A)···H−C(17) in salt **4** are 2.522, 2.594, and 2.831 Å, respectively.

2.3. Photophysical Properties of Compounds 1 to 4. The photophysical properties of compounds **1** to **4** were studied in detail using UV−vis absorption spectrophotometer, fluorimeter, and time-correlated single-photon counting (TCSPC) techniques. Figure 4 shows the UV−vis absorption spectra of compounds **1** to **4**. The absorption spectrum of compound **1** shows a strong peak at 232 nm, and a relatively weak peak at 275 nm, and another weak peak at about 368 nm with a shoulder at

https://doi.org/10.1021/acsomega.1c00679
ACS Omega 2021, 6, 10318−10332

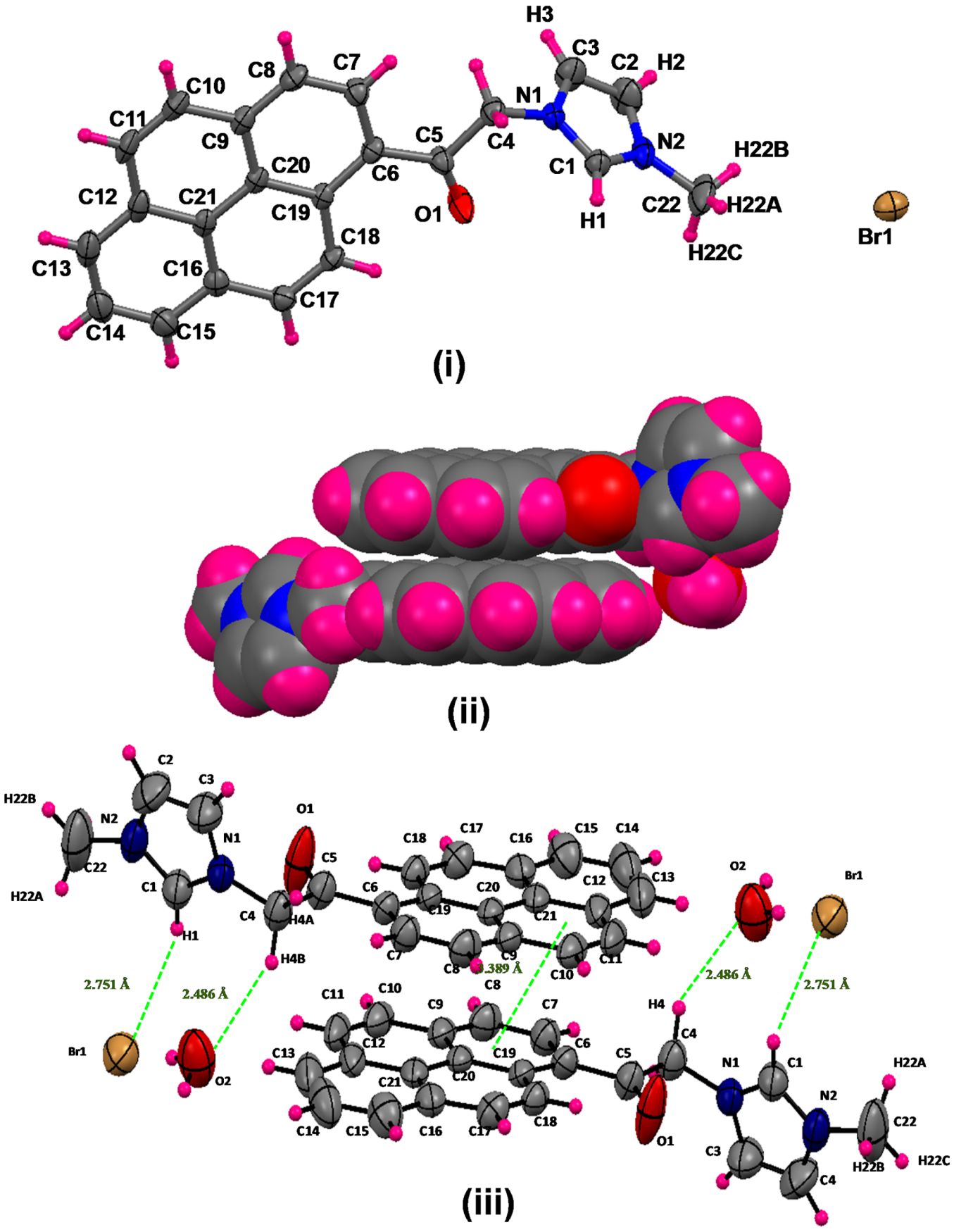

Figure 1. (i) Monomer, (ii) space filling model, and (iii) intermolecular short contacts of salt **1**. Water molecules have been omitted for clarity. Thermal ellipsoids are shown at 50% probability.

https://doi.org/10.1021/acsomega.1c00679
ACS Omega 2021, 6, 10318−10332

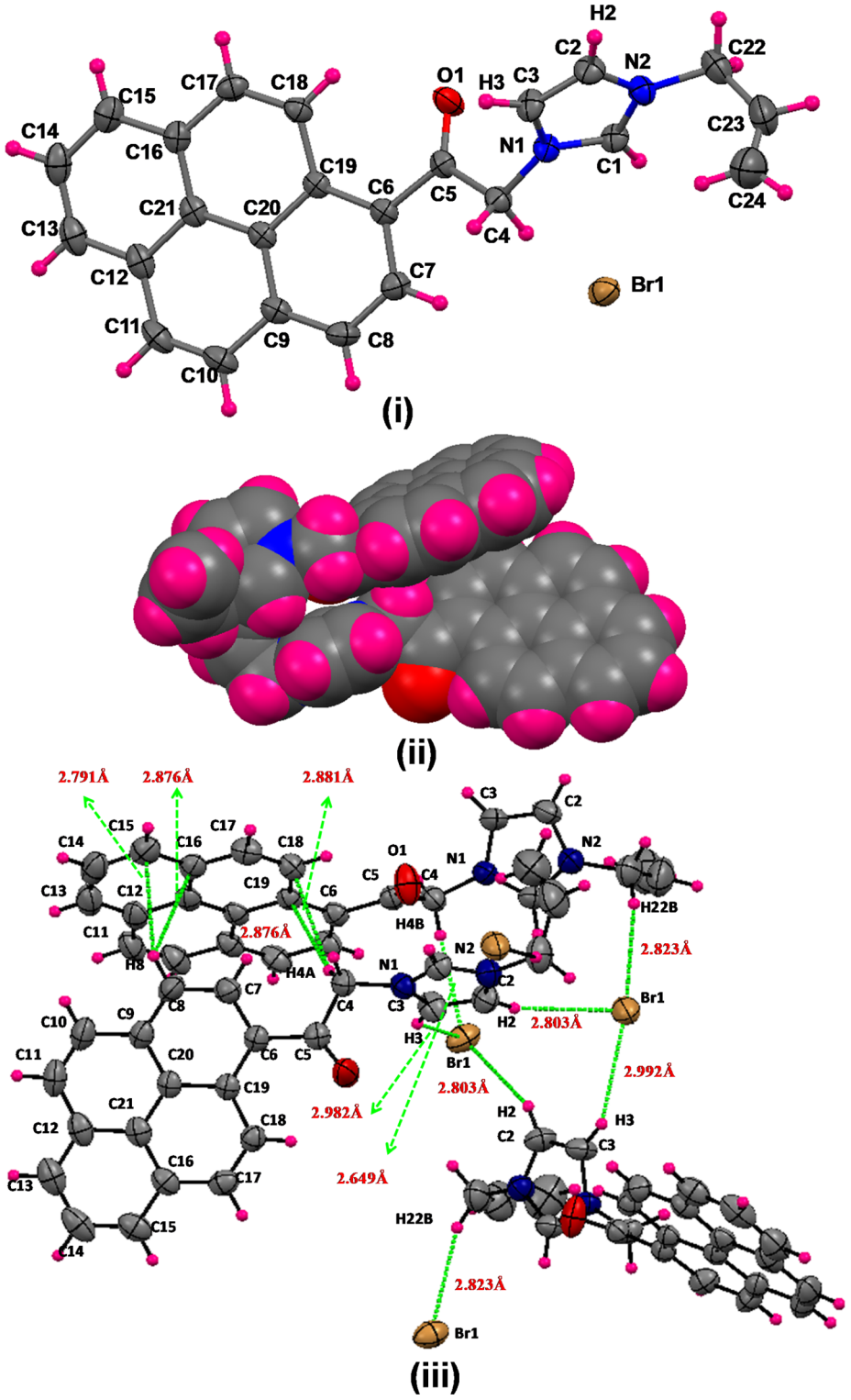

Figure 2. (i) Monomer, (ii) space filling model, and (iii) hydrogen bonding network of salt **3**. Thermal ellipsoids are shown at 50% probability.

395 nm. It may be noteworthy that the methyl imidazolium moiety directly attached to the pyrene molecule (**MeIm**$^{+}$,BF4^{-}) reported by Robillard *et al.*[47] also exhibits a similar absorption peak obtained for compound **1** except for the longer wavelength absorptions which are significantly blue-shifted as compared with compound **1**. This can be justified by the absence of a keto methylene (−CO−CH_2−) spacer between the pyrene ring and the methyl imidazolium group as in the case of compound **1**. There is no notable difference among the structures and positions of the absorption spectra of compounds **1** to **4**. Furthermore, they exhibit similar extinction coefficients in the order of 10^4 M^{-1} cm^{-1} (Figures S11−S14 in Supporting Information). The magnitude of the extinction coefficients conveys that the transitions may be originated from $\pi \rightarrow \pi^*$ transitions. The parameters derived from the absorption spectra of compounds **1** to **4** are summarized in Table S1.

https://doi.org/10.1021/acsomega.1c00679
ACS Omega 2021, 6, 10318−10332

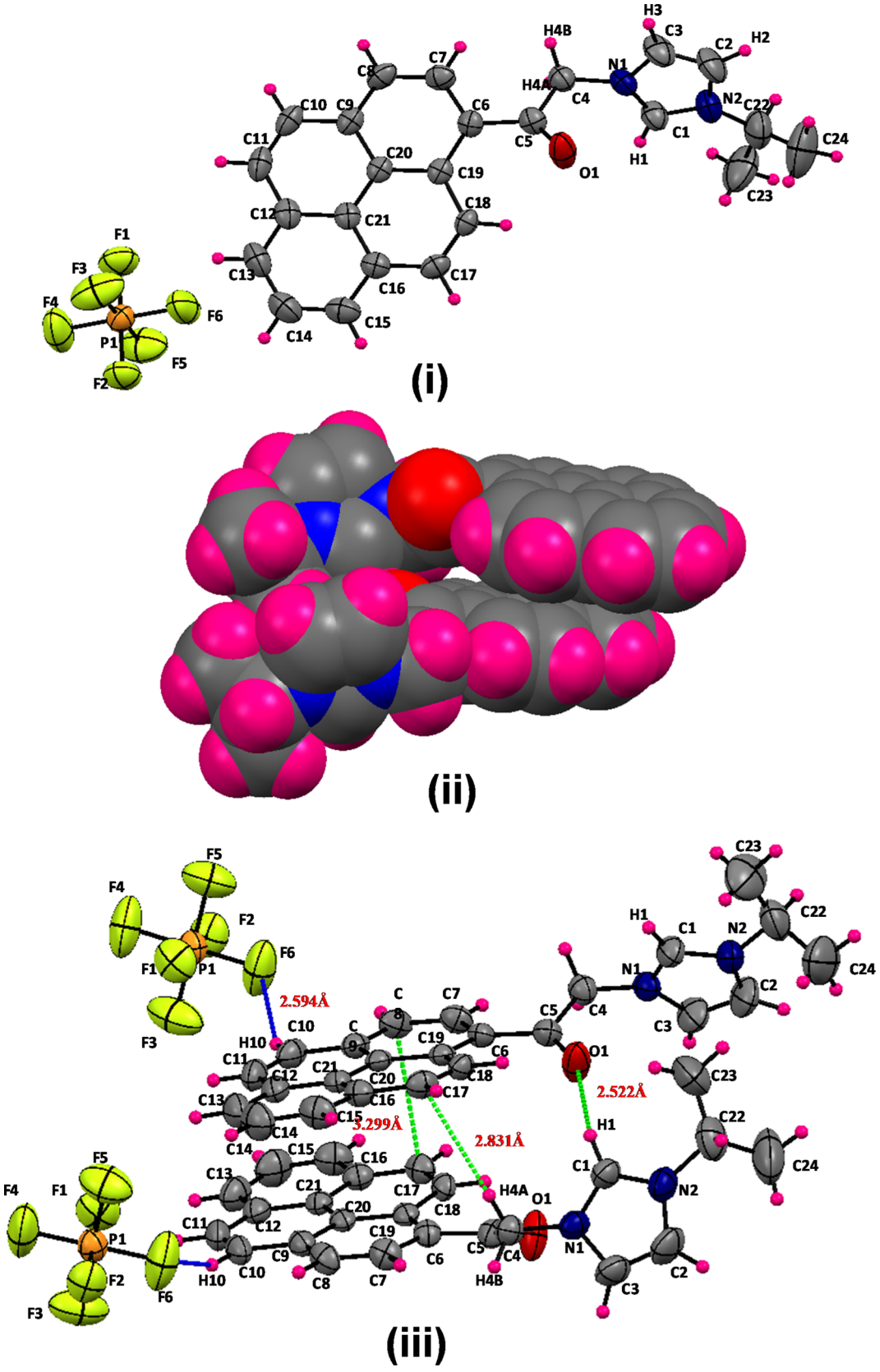

Figure 3. (i) Monomer, (ii) space filling model, and (iii) intermolecular short contacts of salt **4**. Thermal ellipsoids are shown at 50% probability.

Compounds **1** to **4** exhibit bright fluorescence under UV (365 nm) irradiation, as shown in Figure S15. The peak-normalized fluorescence spectra of compounds **1** to **4** are shown in Figure 5. The inset of Figure 5 shows an intense blue emission of the representative compound **4** on excitation at 380 nm. Two emission regions were observed for all the four pyrene derivatives with varying relative intensity. The emission wavelengths are given in Table S2 in the Supporting

https://doi.org/10.1021/acsomega.1c00679
ACS Omega 2021, 6, 10318−10332

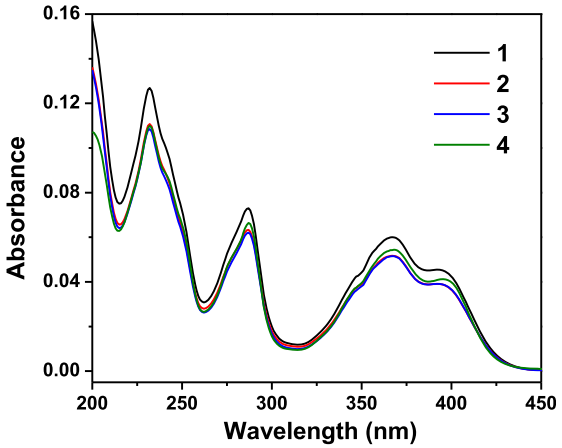

Figure 4. Absorption spectra of compounds **1** to **4** at the concentration of 3.33 μM in aqueous or semi-aqueous media.

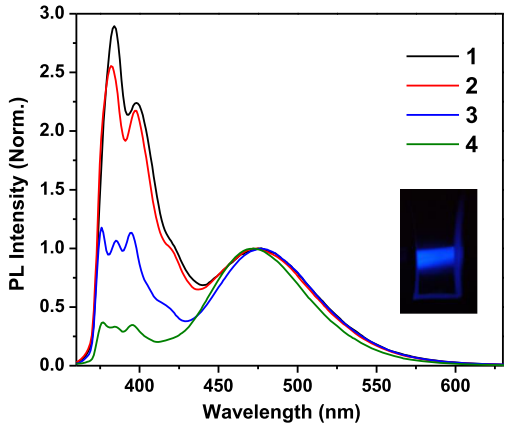

Figure 5. Emission spectra (normalized at longer wavelength peak) of compounds **1** to **4** at the concentration of 3.33 μM in aqueous or semi-aqueous media (λ_{ex}: 340 nm).

Information. The percentage fluorescence quantum yields (ϕ_f) of compounds **1** to **4** were found to be 1.95, 2.18, 2.09, and 20.7 respectively. It is interesting to note that the ϕ_f of **4** is almost ten-folds higher than its bromide analogue, that is, compound **2**. This may be due to the so-called "heavy atom effect"[48] caused by the bromide anion. The pyrene molecules are likely to be affected by the heavy atom effect of halogens.[49] The heavy atom effect is a fluorescence quenching process that promotes non-radiative intersystem crossing to convert a vibrationally active S1 state to an isoenergetic triplet state T1. In compound **4**, the heavy atom effect is nullified by the replacement of a bromide anion by a PF_6 anion. Consequently, the ϕ_f of **4** increased dramatically. Pyrene molecules are well-known for the formation of emissive "excimers" at their excited state.[50] Hence, the structured emission bands observed from about 370 to 420 nm region are assigned to the "monomer" emission originated from the "locally excited" pyrene derivatives while the structureless bands observed from about 430 to 580 nm are attributed to the "excimer" emission. Generally, the excimer emissions are of two types: "dynamic excimer" or "Birks excimer" (E*) and "static excimer" (D*). According to Birks, the dynamic excimers are formed at the electronically excited state when a locally excited pyrene molecule forms a complex with a ground state pyrene molecule.[51] There are also instances where an excimer-like emission is observed, but there is no evidence that the pyrenes are separated when the light is absorbed.[52] These excited species are referred to as "static excimers" by several scientists as this emission strongly resembles the pyrene excimer emission.[52] These excimers can be distinguished from the photophysical parameters as described by Winnik.[52] Broadening of absorption spectra of pyrene derivatives often indicates the formation of preassociated pyrenes. Apart from that, the ratio (P_A) of the absorbance of the most intense band to that of the adjacent minimum intensity band at shorter wavelength will usually be > 3.0 for the locally excited (^1L_a) 1-substituted pyrene molecule in the absence of preassociation. This value decreases depending on the extent of the preassociation of pyrene molecules. For compounds **1** to **4**, the P_A values were found to be 1.72, 1.72, 1.77, and 1.63, respectively, which indicates the pyrene preassociation. It is noteworthy that the P_A values are in accordance with the crystal structure data obtained from single crystal XRD studies. The increasing order of the interactions between two pyrene moieties in compounds **1**, **3**, and **4** as obtained from their corresponding single crystal XRD data (Figures 1−3) is noted to be **3** < **1** < **4**. The same order reflects in the P_A values of the compounds **1**, **3**, and **4**, that is, the preassociation is slightly higher in compound **4** while it is comparatively lower in compound **3**. The formation of ground-state preassociation of pyrenes can further be ascertained from the excitation spectra of the pyrene compounds monitored at

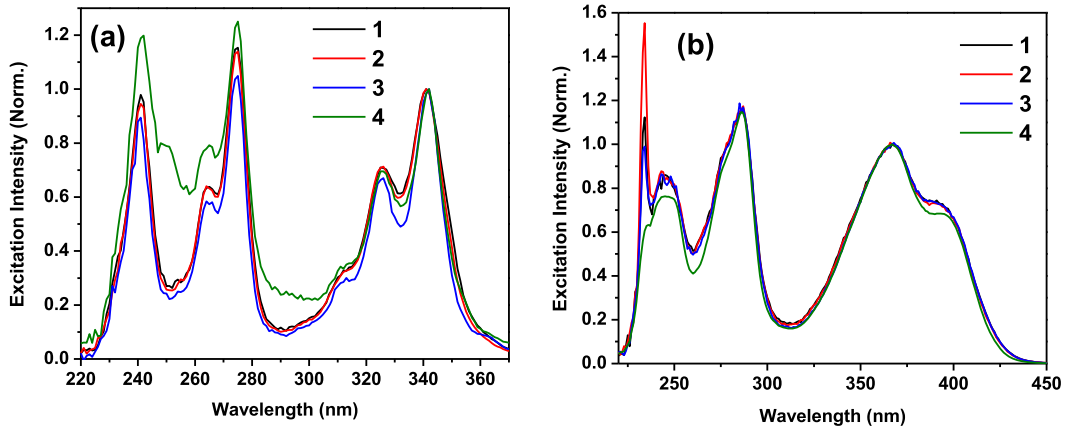

Figure 6. Excitation spectra (normalized at longer wavelength peak) of compounds **1** to **4** in aqueous or semi-aqueous media, monitored at (a) monomer emission wavelength and (b) excimer emission wavelength.

https://doi.org/10.1021/acsomega.1c00679
ACS Omega 2021, 6, 10318−10332

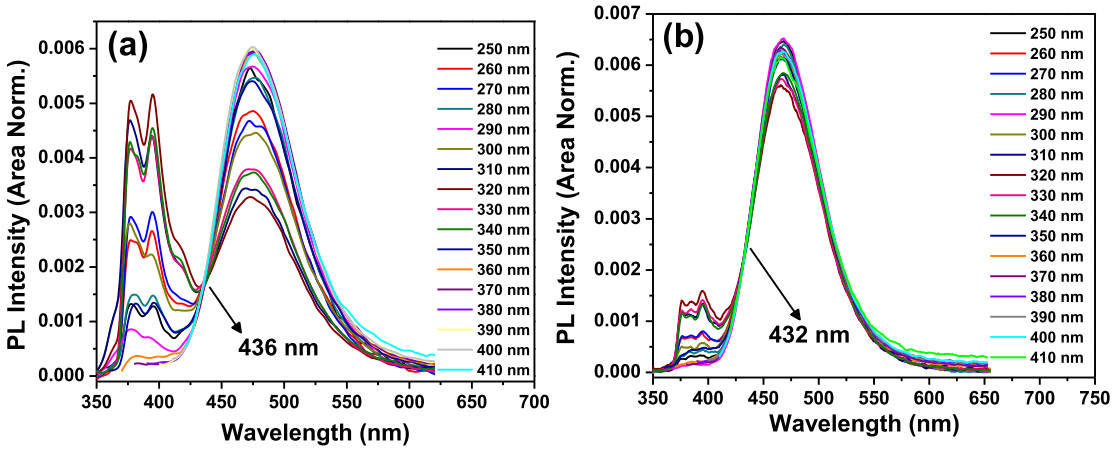

Figure 7. ERANES spectra constructed for (a) compound **2** (isoemissive point: 436 nm) and (b) compound **4** (isoemissive point: 432 nm).

the monomer and excimer emission maxima. These excitation bands may not be superimposed in the case of preassociation. Furthermore, the D* band will be red-shifted and comparatively broader compared to that of the E* band. These features are clearly observed in the excitation spectra of compounds **1** to **4** monitored at monomer and excimer emission wavelengths, as shown in Figure 6a,b and Table S3. The 2D fluorescence contour topographical maps of compounds **1** to **4** are shown in Figures S16−S19 (Supporting Information) for more clear understanding.

Recently, Selvaraju *et al.*[53] have proposed excitation-resolved area-normalized emission spectroscopy (ERANES) as a new steady-state fluorescence technique for the analysis of heterogeneous fluorescence. According to them, the total number of ground-state fluorophores present in a mixture could be identified by adding the numeral "1" to the total number of isoemissive points obtained in the ERANES (isoemissive points + 1). We have applied this technique to further confirm the presence of D* in compounds **1**−**4**. We should observe a single isoemissive point if the excimer is of static nature. On the other hand, the isoemissive point could not be observed if the excimer is of dynamic nature. Obvious single isoemissive points were observed for all the four compounds on the ERANES analysis which confirmed the presence of D* in all the four compounds. The ERANES spectra constructed for compounds **2** and **4** are given in Figure 7a,b, respectively. Similarly, the ERANES spectra constructed for the compounds **1** and **3** are shown in Figure S20a,b respectively.

To further substantiate the formation of D*, fluorescence lifetime measurements were performed for compounds **1** to **4** to observe whether the growth of the excimer appeared in the fluorescence decay of excimer emission (Figure 8). The compounds were excited at 375 nm using a light-emitting diode excitation source (pulse duration: <1 ns), and the excimer emission was monitored for example at 475 nm for compound **1**. The resulting decay profiles were best fitted with a bi-exponential function, and the average lifetimes were calculated to be 0.58, 0.58, 0.52, and 0.70 ns for compounds **1** to **4**, respectively. The fitted parameters are shown in Table S4 in the Supporting Information. The absence of any growth formation in the fluorescence decay profiles, further evince the absence of a dynamic excimer. Hence, the observed excimer emission should be originated from the static excimer.

We have also performed the fluorescence lifetime measurements of compounds **1** to **4** at the monomer emission by exciting

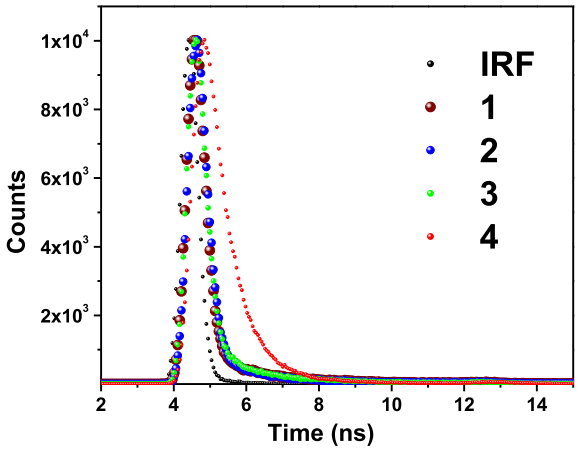

Figure 8. Fluorescence lifetime decay profiles of compounds **1** to **4** monitored at excimer emission (λ_{ex}: 375 nm); IRF: instrument response function.

the compounds using a 295 nm light-emitting diode excitation source (pulse duration: <1 ns). The resulting decay profiles were best fitted with a tri-exponential function and yielded the mean lifetimes of 18.69, 21.61, 12.11, and 11.76 ns for compounds **1** to **4**, respectively. The decay profiles and the fitted parameters are shown, respectively, in Figure S21 and Table S5 in the Supporting Information.

2.4. Solid-State Emission Behavior of Compounds 1 to 4. An interesting feature of compounds **1** to **4** is their solid-state emission property, as shown in Figure S22, in which compounds **1** to **4** in their solid-state were exposed to daylight and UV (365 nm) light. The solid-state emissions are visible for compounds **2** and **4**. Solid-state emission spectra were recorded for compounds **1** to **4** and are shown in Figure 9. Compound **1** exhibits a structured emission band while compounds **2** to **4** exhibit structureless bands. The emission bands of compounds **2** and **4** show a clear red shift from their solution-state emission bands. This may be probably due to the strong interactions between adjacent pyrene molecules in the π-stacks as observed from the single crystal XRD data. The monomer emission bands are not observed in the solid-state emission spectra of compounds **1** to **4** (the monomer emission regions are not shown in the solid-state emission spectra Figure 9). Table S2 compares the solid-state emission maxima with that of the solution-state emission maxima of compounds **1** to **4**.

https://doi.org/10.1021/acsomega.1c00679
ACS Omega 2021, 6, 10318−10332

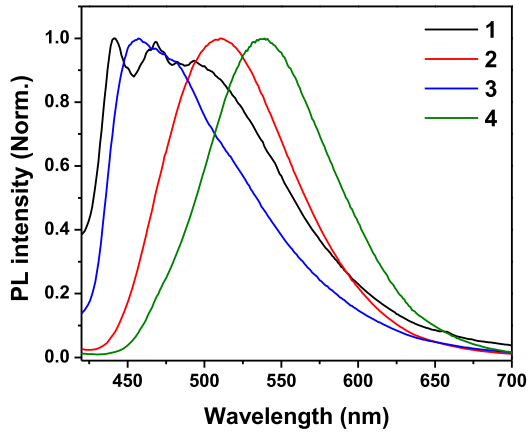

Figure 9. Peak normalized solid-state emission spectra of compounds **1** to **4**

Compounds **1** to **4** exhibit bright yellow and red color emissions when exposed to a blue and green light, respectively. These images were viewed using a fluorescence microscope (LEICA DMIRE2) and captured by a smartphone (brand: oppo, model: realme 1, camera pixel: 13 MP). The image for compound **4** is shown in Figure 10a,b to represent this observation. Then, the compounds were viewed through a fluorescence microscope, and the fluorescence images were recorded at various emission wavelengths. Figure 10c,d shows the green and red emissions of compound **4** while the yellow emission shown in Figure 10e is an overlaid image of Figure 10c,d (scale bar: 153 μm). Similar images showing the solid-state emissions of compounds **1** to **3** are presented in Figure S23 (a–e), Figure S24 (a–e), and Figure S25 (a–e) in the Supporting Information. It is discussed in the previous section that all the compounds **1** to **4** exist as monomers and static excimers in their ground state itself. This ground state heterogeneity may be the reason for the excitation light dependency of the emission wavelength that is observed for the compounds **1** to **4**.

2.5. Decipherment of Latent Fingerprints Using a Fingerprint Powder Formulation Based on Compound 4.

The excellent solid-state emission property of compounds **1** to **4** makes them effective candidates for many applications such as light-emitting display devices, scintillation counters, phosphors, bioimaging, and so forth.[41,42] One of the areas where the solid-state emissive chromophores find their effective application is the forensic investigation of latent fingerprints.[43] The conventional non-emissive fingerprint powders can be applied only when there is a good contrast between the color of the fingerprint powders and the background surfaces. In many instances such as the latent fingerprints deposited on multicolor surfaces, it is difficult to choose a suitable fingerprint powder to detect, develop, and lift the latent fingerprints. In this situation, the luminescent fingerprint powders are more effective as the fingerprints developed by them can easily be viewed using a suitable excitation light source and photographed for documentation.

In this context, we have attempted to formulate a luminescent fingerprint powder based on compound **4** and presented our preliminary results here. The compound **4** is mixed with neutral aluminum oxide G, TLC grade (Sisco Research Laboratories Pvt. Ltd.) in 1:20 w/w ratio, and thoroughly ground in a mortar by a pestle to yield a homogenous mixture. The main purpose of using neutral alumina is to serve as a base material for a smooth application of the powder on latent fingerprints. The powder technique for the revelation of latent fingerprints largely relies on the selective physical adherence of the fingerprint powder on the

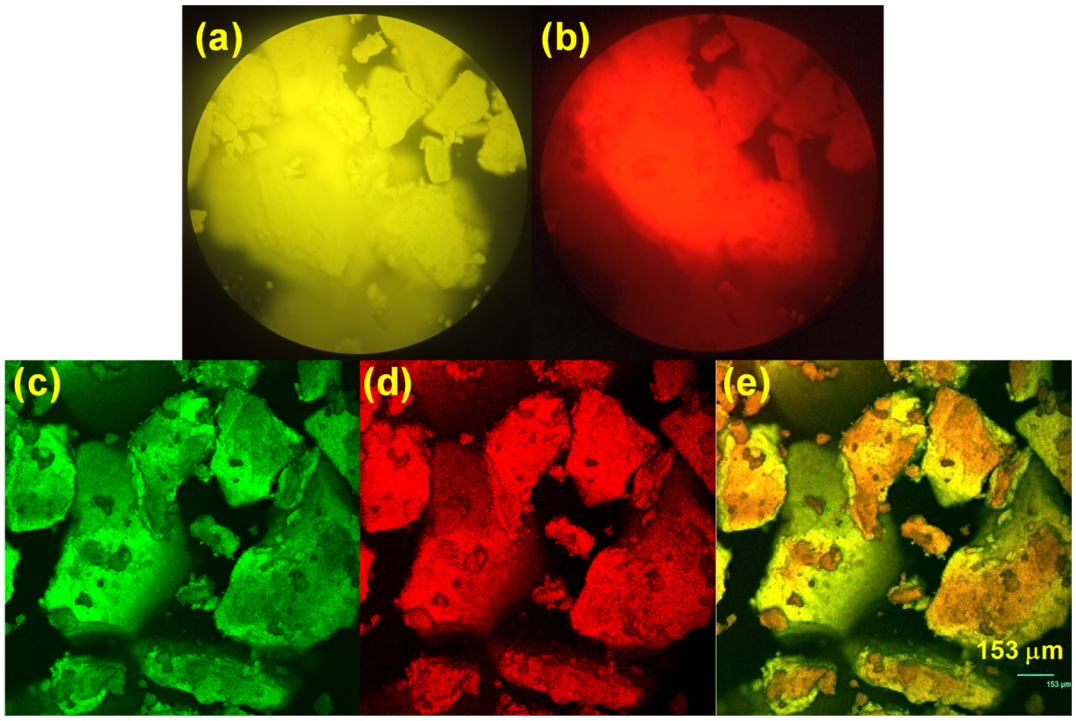

Figure 10. Solid-state emissions of compound **4** viewed through a confocal microscope on exposure to (a) blue and (b) green lights; solid-state emissions of compound **4** recorded using a confocal microscope on excitation of 488 nm laser and the emission monitored at (c) green and (d) red regions. (e) Overlaid image of c and d (scale bar = 153 μm).

https://doi.org/10.1021/acsomega.1c00679
ACS Omega 2021, 6, 10318−10332

latent fingerprints. The TLC grade alumina may help in the adhesion of the fingerprint powder as it contains a binder (usually gypsum) in its formulation.[54] The formulated fingerprint powder exhibits a bright yellow color emission on exposure to UV (365 nm) light, as shown in Figure S26a,b.

The fingerprint powder was applied on the latent fingerprint deposited on a microscopic glass plate by a volunteer and pressed gently. The excess powders were removed by a tapping and blowing method. The resulting developed fingerprints were photographed under UV light (365 nm), and one of them is shown in Figure 11 as a representative image. The minutiae

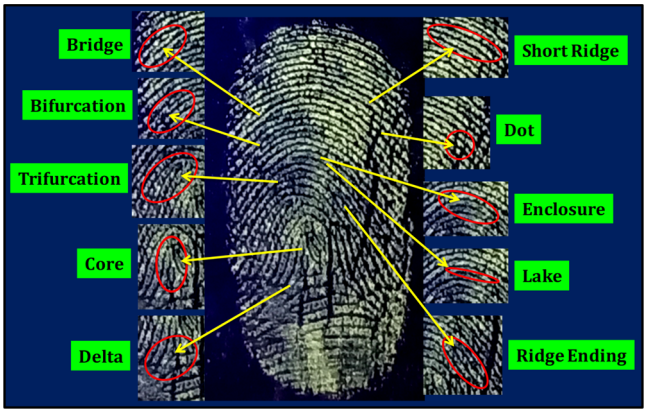

Figure 11. Minutiae features of the fingerprints developed using compound **4**-based fingerprint powder and exposed to UV light (365 nm).

features such as bridge, bifurcation, trifurcation, core, delta, short ridge, dot, enclosure, lake, and ridge ends can be observed in Figure 11. Hence, it is clear that "level 2" information can be extracted from the fingerprints developed by this fingerprint powder. The fingerprint characteristics can be divided into three levels.[55] Level 1 refers to the general pattern formed by the flow of ridges on the papillary surface, singular points, and types. These are macro details of a fingerprint. The level 2 features are due to major deviations on the ridge patterns such as bi/trifurcations, ridge crossovers, islands, spur, and so forth. These discrete points are referred to as "minutiae" or "Galton characteristics". On the other hand, the level 3 features include all dimensional attributes of the ridge path deviation, such as alignment and morphology of each ridge units, shapes and relative positions of pores, and so forth. The pore morphological features are micro-level details of a fingerprint. It is worth noting that a large number of sweat pores are visible all over Figure 11 especially around the core area. Hence, these fingerprints could also provide "level 3" information.

In this context, the fingerprint in Figure 11 was digitally enlarged at a selected area around its core region and the contrast was digitally increased to 30%. The resulting image is shown in Figure S27 which reveals the presence of many pores on the friction ridges. From the image, the relative positions of the pores and the pore morphology such as its shape and relative size can be extracted.

Apart from these features, an excellent observation is made in the UV-developed fingerprint *viz.* the appearance of empty narrow paths, as marked in Figure S28b,c. These features are found due to the presence of wrinkles on the volunteer's finger (Figure S28a) which are exactly traced on its developed fingerprint. This is an excellent individual characteristic, and these kinds of features are rarely observed in forensic examinations. These individual features ease the job of a forensic examiner on the identification of the fingerprints.

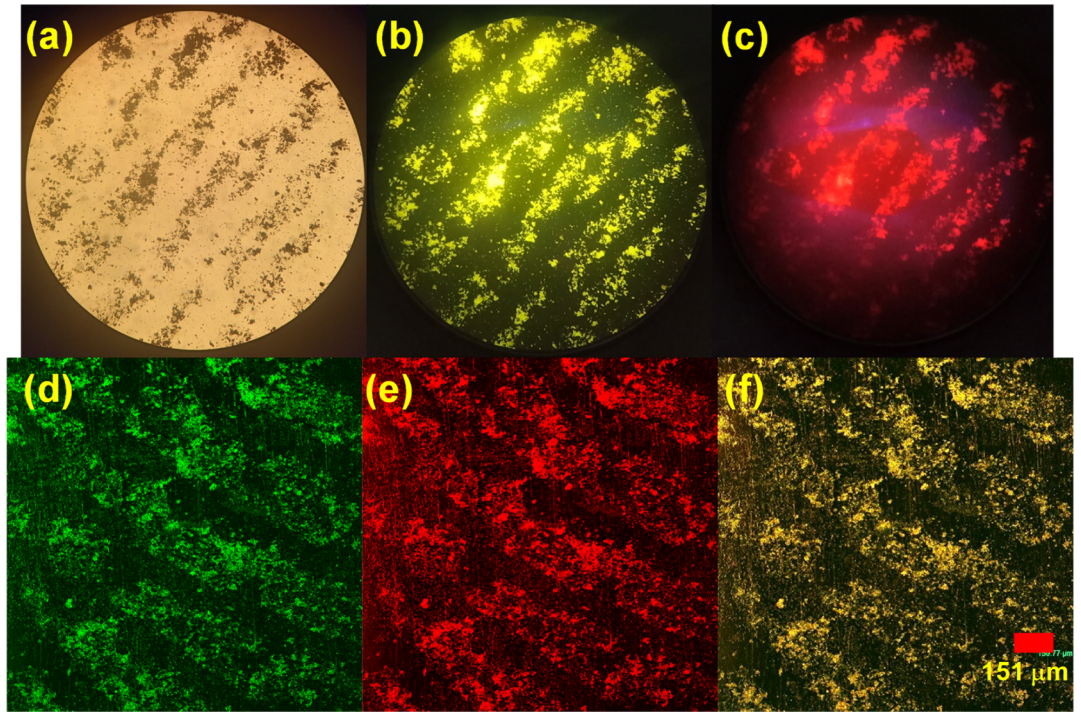

Figure 12. Fingerprints developed using compound **4**-based fingerprint powder viewed through a confocal microscope on exposure to (a) bright field (b) blue and (c) green lights; fingerprints developed using compound **4**-based fingerprint powder recorded using a confocal microscope on excitation of 488 nm laser and the emission monitored at (d) green and (e) red regions. (f) Overlaid image of d and e (scale bar = 151 μm).

https://doi.org/10.1021/acsomega.1c00679
ACS Omega 2021, 6, 10318−10332

Figure 11 also reveals a very good contrast between the friction ridges and the furrow. To explore the micro-level details more clearly, we have viewed the developed fingerprint using a confocal microscope after exciting the fingerprints with blue and green lights. The resulting images are presented in Figure 12a−f. Figure 12a is the bright field image of the developed fingerprints while the images in Figure 12b,c are those exposed under blue and green lights, respectively. Then, the fluorescence images of the developed fingerprints were recorded at various emission wavelengths. Figure 12d,e shows green and red emissions. On the other hand, the yellow emission shown in Figure 12e is an overlaid image of Figure 12d,e (scale bar: 151 μm). The sweat pores can also be visualized (hollow spaces on the ridgelines) well in Figure 12a−f. The selective adherence of the fingerprint powder on the ridges rather than the furrow is also revealed well from Figures 11 and 12a−f. The fingerprints should be deposited on various porous and non-porous surfaces to further investigate the efficiency of the fingerprint powders formulated based on compounds **1** to **4** and the same will be studied separately.

3. CONCLUSIONS

Water-soluble pyrene-tagged imidazolium salts have been synthesized in good yield. The obtained imidazolium salts (**1**−**4**) show remarkable photo and thermal stabilities under various conditions. The structures of **1**, **3**, and **4** were confirmed by single-crystal X-ray diffraction analysis. The solid-state packing and space-filling model of **1** and **4** shows that pyrene moieties are closely packed with a weak $\pi-\pi$ interaction. Moreover, weak inter and intramolecular interactions were present in the closely packed three-dimensional framework. Detailed photophysical investigation was done for compounds **1** to **4**. In the solution state, the imidazolium salts emit an intense blue color. Surprisingly, in the solid-state, all the four compounds show yellow and red color emissions based on the excitation wavelength. The solid-state emissions were examined by a fluorescence microscope. To exploit the solid-state luminescence of the synthesized compounds toward forensic applications, we have formulated a fingerprint powder with compound **4** as a representative compound. The resulting powder is used to develop the latent fingerprints. The fingerprints exhibit various color emissions depending on the excitation wavelength. The minutiae features are visible in daylight as well as in UV light (365 nm) conditions. Our preliminary studies show that the fingerprint powder can be successfully applied to develop the latent fingerprints in forensic applications.

4. MATERIALS AND METHODS

4.1. Chemicals and Reagents. All manipulations were carried out under a N_2 atmosphere using standard Schlenk techniques. The solvents were purchased from commercial sources and purified according to standard procedures.[56] Potassium hexafluorophosphate, 1-(bromoacetyl)pyrene, *N*-methylimidazole, and *N*-allylimidazole were purchased from Sigma-Aldrich. *N*-isopropyl imidazole was obtained from TCI Chemicals (India) Pvt. Ltd. 1-*N*-methyl-3-(2-oxo-2-(pyren-1-yl)ethyl)-imidazolium bromide (**1**) was prepared as reported.[44] [1-*N*-isopropyl-3-(2-oxo-2-(pyren-1-yl)ethyl)-imidazolium bromide (**2**), 1-*N*-allyl-3-(2-oxo-2-(pyren-1-yl)ethyl)-imidazolium bromide (**3**) and 1-*N*-isopropyl-3-(2-oxo-2-(pyren-1-yl)ethyl)-imidazolium hexafluorophosphate (**4**) were newly synthesized by modified procedures. Thin-layer chromatography (TLC) was performed on Merck 1.05554 aluminum sheets precoated with silica gel 60 F254, and the spots were visualized with UV light at 254 nm or under iodine.

4.2. Instruments Used for Characterization. Infrared spectra of the compounds were recorded and identified using a Bruker, VERTEX 70 Fourier transform infrared spectrometer at ATR mode. ^{1}H (400 MHz) and ^{13}C (75.47 MHz) NMR spectra were taken in DMSO-d_6 at room temperature with a Bruker AVANCE III HD instrument, and ^{19}F (60 MHz) NMR spectra were taken in DMSO-d_6 at room temperature with a Spinsolve 60 carbon benchtop NMR instrument. Chemical shifts are given relative to tetramethylsilane and have been referenced to the solvent resonances as internal standards. Melting points were determined in open capillary tubes on a Technico microheating table. UV−vis absorption spectra were recorded with a Cary 100 Bio UV−visible double beam spectrophotometer. Fluorescence, excitation, and 3D contour spectra were recorded by a HORIBA JOBIN YVON Fluoromax 4P spectrofluorometer. ERANES were constructed from the excitation-resolved fluorescence spectra and recorded using a PerkinElmer MPF-44B fluorescence spectrophotometer. The fluorescence decay measurements were carried out using a TCSPC technique using 375 and 295 nm light-emitting diodes (LEDs) as the excitation sources. The TCSPC data analyses were carried out by the software provided by IBH (DAS-6), which is based on the deconvolution technique using iterative nonlinear least-squares methods. The quality of the fit is normally identified by the reduced χ^2 value. The relative fluorescence quantum yield (QY) was calculated by comparing the integrated PL intensities (excited at 355 nm) and the absorbance values of the pyrene-tagged NHC-derivatives at 355 nm with those of the reference quinine sulfate. The ridge spacing and the sweat pore morphology of alumina developed fingerprints were viewed under a fluorescence microscope (LEICA DMIRE2). 10× objectives were used to view the fingerprints.

The crystal structures of **1**, **3**, and **4** were recorded using a Gemini Ultra Oxford Diffraction automatic diffractometer. The single crystals of compounds **1**, **3**, and **4** were obtained from the reaction mixtures of the complexes at room temperature. A suitable single crystal of **1**, **3**, and **4** was selected and mounted on the glass fibers. Graphite monochromated Mo Kα radiation (λ = 0.71073 Å) was used throughout the experiment. The crystal was kept at 298 K during data collection. The absorption corrections were performed by the multiscan method. Corrections were made for Lorentz and polarization effects. The structures were solved by direct methods using the program SHELXS.[57] Refinement and all further calculations were carried out using SHELXL.[57] The H atoms were included in calculated positions and treated as riding atoms using the SHELXL default parameters. The non-hydrogen atoms were refined anisotropically using weighted full-matrix least-squares on F2. Atomic scattering factors were incorporated into the computer programs.

4.3. Synthesis of 1-*N*-Methyl-3-(2-oxo-2-(pyren-1-yl)-ethyl)-imidazolium Bromide (1). A mixture of 1-(bromoacetyl)pyrene (1.13 g, 3.50 mmol) and 1-methylimidazole (0.3 mL, 3.50 mmol) in acetonitrile (8 mL) was refluxed for 24 h under a N_2 atmosphere. After completion of the reaction, the solvent was evaporated under vacuum, and then the resulting solid was washed thrice with acetone. Compound **1** was obtained as pale yellow powder. The single crystal of **1** was grown by slow evaporation of the concentrated solution of the

https://doi.org/10.1021/acsomega.1c00679
ACS Omega 2021, 6, 10318−10332

compound in the methanol/acetone (1:1) mixture at room temperature. Yield 92% (based on 1-(bromoacetyl)pyrene). M.p.: 264−266 °C. Anal. calcd. for $C_{22}H_{17}N_2OBr$, (405.29): C, 65.20; H, 4.23; N, 6.91%; found, C, 65.07; H, 4.12; N, 6.79%. FT-IR (cm^{-1}, neat): ν(C═O) 1678, ν(C−N) 1591. ^{1}H NMR (400 MHz, DMSO-d_6): δ 9.27 (s, 1H, NCHN), 9.04−9.02 (d, 1H, J = 9.6 Hz, ArH), 8.83−8.81 (d, 1H, J = 8 Hz, ArH), 8.51−8.42 (m, 5H, ArH), 8.41−8.40 (d, 1H, J = 4.4 Hz, ArH), 8.33−8.19 (t, 1H, ArH), 7.90−7.88 (d, 2H, J = 10.4 Hz, $CH_{imidazole}$), 6.36 (s, 2H, $-NCH_2$), 4.04 (s, 3H, $-NCH_3$). ^{13}C NMR (100 MHz, DMSO-d_6): δ 194.60 (C═O), 138.38 (NCHN), 134.86 (ArC), 131.03 (ArC), 130.84 (ArC), 130.74 (ArC), 130.28 (ArC), 129.88 (ArC), 128.04 (ArC), 127.64 (ArC), 127.12 (ArC), 124.97 (ArC), 124.57 (ArC), 124.49 (ArC), 123.81 ($CH_{imidazole}$), 123.65 ($CH_{imidazole}$), 57.61 ($-NCH_2$), 36.53 ($-NCH_3$).

4.4. Synthesis of 1-*N*-Isopropyl-3-(2-oxo-2-(pyren-1-yl)ethyl)-imidazolium Bromide (2). A mixture of 1-(bromoacetyl)pyrene (1.13 g, 3.50 mmol) and 1-isopropylimidazole (0.4 mL, 3.50 mmol) in acetonitrile (8 mL) was refluxed for 24 h under a N_2 atmosphere. After completion of the reaction, the solvent was evaporated under *vacuum*, and then the resulting solid was washed thrice with acetone. Compound **2** was obtained as pale yellow powder. Yield 90% (based on 1-(bromoacetyl)pyrene). M.p.: 258−261 °C. Anal. calcd for $C_{24}H_{21}N_2OBr$, (433.34): C, 66.52; H, 4.88; N, 6.46%; found, C, 66.40; H, 4.72; N, 6.58%. FT-IR (cm^{-1}, neat): ν(C═O) 1680, ν(C−N) 1594. ^{1}H NMR (400 MHz, DMSO-d_6): δ 9.42 (s, 1H, NCHN), 9.06−9.03 (d, 1H, J = 9.2 Hz, ArH), 8.82−8.80 (d, 1H, J = 8 Hz, ArH), 8.53−8.45 (m, 5H, ArH), 8.43−8.42 (d, 1H, J = 4 Hz, ArH), 8.41−8.20 (t, 1H, ArH), 8.09 (s, 1H, $CH_{imidazole}$), 7.93 (s, 1H, $CH_{imidazole}$), 6.32 (s, 2H, $-NCH_2$), 4.89−4.79 (septet, 1H, −CH), 1.59−1.57 (d, 6H, J = 6.4 Hz, $-CH_3$). ^{13}C NMR (100 MHz, DMSO-d_6): δ 194.55 (C═O), 136.76 (NCHN), 134.90 (ArC), 131.05 (ArC), 130.88 (ArC), 130.74 (ArC), 130.30 (ArC), 129.90 (ArC), 128.01 (ArC), 127.65 (ArC), 127.56 (ArC), 127.15 (ArC), 124.86 (ArC), 124.73 (ArC), 124.51 (ArC), 123.67 ($CH_{imidazole}$), 120.70 ($CH_{imidazole}$), 57.61 ($-NCH_2$), 52.92 (−CH), 22.69 ($-NCH_3$). Unfortunately, we have not yet obtained high-quality single crystals of compound **2** for X-ray diffraction analysis.

4.5. Synthesis of 1-*N*-Allyl-3-(2-oxo-2-(pyren-1-yl)-ethyl)-imidazolium Bromide (3). A mixture of 1-(bromoacetyl)pyrene (1.13 g, 3.50 mmol) and 1-allylimidazole (0.4 mL, 3.50 mmol) in acetonitrile (8 mL) was refluxed for 24 h under a N_2 atmosphere. After completion of the reaction, the solvent was evaporated under *vacuum*, and then the resulting solid was washed thrice with acetone. Compound **3** was obtained as pale yellow powder. The single crystal of **3** was grown by slow evaporation of the concentrated solution of the compound in acetonitrile at room temperature. Yield 89% (based on 1-(bromoacetyl)pyrene). M.p.: 224−227 °C. Anal. calcd for $C_{24}H_{19}N_2OBr$, (431.32): C, 66.83; H, 4.44; N, 6.49%; found, C, 66.71; H, 4.32; N, 6.54%. FT-IR (cm^{-1}, neat):ν(C═O) 1678, ν(C−N) 1591. ^{1}H NMR (400 MHz, DMSO-d_6): δ 9.33 (s, 1H, NCHN), 9.06−9.03 (d, 1H, J = 9.6 Hz, ArH), 8.83−8.81 (d, 1H, J = 8 Hz, ArH), 8.53−8.43 (m, 5H, ArH), 8.42−8.41 (d, 1H, J = 4 Hz, ArH), 8.35−8.20 (t, 1H, ArH), 7.94 (s, 1H, $CH_{imidazole}$), 7.91 (s, 1H, $CH_{imidazole}$), 6.35 (s, 2H, $-NCH_2$), 6.20−6.13 (m, 1H, CH═CH_2), 5.46−5.43 (d, 1H, J = 10 Hz, CHH*trans*), 5.40−5.36 (d, 1H, J = 17.2 Hz, CHH*cis*), 5.06−5.04 (d, 2H, J = 6 Hz, CH_2). ^{13}C NMR (100 MHz, DMSO-d_6): δ 194.55 (C═O), 138.08 (NCHN), 134.39 (ArC), 132.39 (ArC), 131.05 (ArC), 130.87 (ArC), 130.74 (CH═CH_2), 130.30 (ArC), 129.90 (ArC), 128.04 (ArC), 127.65 (ArC), 127.63 (ArC), 127.56 (ArC), 127.15 (ArC), 124.98 (ArC), 124.90 (ArC), 124.72 (ArC), 124.51 (ArC), 123.67 ($CH_{imidazole}$), 122.74 (CH═CH_2), 120.66 ($CH_{imidazole}$), 57.74 ($-NCH_2$), 51.51 (CH_2).

4.6. Synthesis of 1-*N*-Isopropyl-3-(2-oxo-2-(pyren-1-yl)ethyl)-imidazolium Hexafluorophosphate (4). Since we were not successful in obtaining high-quality crystals of compound **2**, we have performed anion metathesis reaction on compound **2** to produce high-quality crystals of 1-*N*-isopropyl-3-(2-oxo-2-(pyren-1-yl)ethyl)-imidazolium hexafluorophosphate (**4**). The synthetic procedure is briefly given as follows. 1-*N*-isopropyl-3-(2-oxo-2-(pyren-1-yl)ethyl)-imidazolium bromide (**2**) (0.1 g, 0.26 mmol) dissolved in hot water (5 mL) was added to an aqueous solution of KPF_6 (0.09 g, 0.52 mmol) (2 ml) under constant stirring. A bright yellow precipitate was formed immediately, and then the reaction mixture was stirred for 8 h at room temperature. The precipitate was filtered and washed with water and methanol to get a crude product. The resultant solid was dissolved in acetone, dried over sodium sulfate, and filtered, and the solvent was evaporated under reduced pressure to get an analytically pure compound **4**. The single crystal of **4** was grown by slow evaporation of the concentrated solution of the compound in acetonitrile at room temperature. Yield 82% (based on **2**). M.p.: 182−184 °C. Anal. calcd. for $C_{24}H_{21}N_2OPF_6$, (498.40): C, 57.84; H, 4.25; N, 5.62%; found, C, 57.69; H, 4.16; N, 5.72%. FT-IR (cm^{-1}, neat): ν(C═O) 1681, ν(C−N) 1595. ^{1}H NMR (400 MHz, DMSO-d_6): δ 9.33 (s, 1H, NCHN), 9.07−9.05 (d, 1H, J = 9.6 Hz, ArH), 8.80−8.77 (d, 1H, J = 8.4 Hz, ArH), 8.53−8.45 (m, 5H, ArH), 8.44−8.43 (d, 1H, J = 4.4 Hz, ArH), 8.42−8.21 (t, 1H, ArH), 8.06 (s, 1H, $CH_{imidazole}$), 7.89 (s, 1H, $CH_{imidazole}$), 6.26 (s, 2H, $-NCH_2$), 4.88−4.78 (septet, 1H, −CH), 1.59−1.58 (d, 6H, J = 6.8 Hz, $-CH_3$). ^{13}C NMR (100 MHz, DMSO-d_6): δ 194.48 (C═O), 136.74 (NCHN), 134.93 (ArC), 131.05 (ArC), 130.91 (ArC), 130.78 (ArC), 130.31 (ArC), 129.93 (ArC), 127.98 (ArC), 127.69 (ArC), 127.65 (ArC), 127.59 (ArC), 127.17 (ArC), 124.98 (ArC), 124.88 (ArC), 124.72 (ArC), 124.53 (ArC), 123.67 ($CH_{imidazole}$), 120.69 ($CH_{imidazole}$), 57.54 ($-NCH_2$), 52.94 (−CH), 22.86 ($-NCH_3$). ^{19}F NMR (60 MHz, DMSO-d_6): δ −62.21 (PF_6), −74.46 (PF_6).

■ ASSOCIATED CONTENT

Supporting Information

The Supporting Information is available free of charge at https://pubs.acs.org/doi/10.1021/acsomega.1c00679.

IR and NMR spectra of compounds **1** to **4**; extinction coefficients, fluorescence contour maps, and lifetime decay profiles of compounds **1** to **4**; ERANES spectra constructed for the compounds **1** and **3**; tables showing the parameters derived from photophysical investigation; images pertaining to the solution and solid-state emissions of compounds **1** to **4**; images showing the solid-state emission of compounds **1** to **4** on the exposure of blue and green lights; images of the fingerprint powder formulation based on compound **4**; and images of fingerprints developed using compound **4** (PDF)

https://doi.org/10.1021/acsomega.1c00679
ACS Omega 2021, 6, 10318−10332

AUTHOR INFORMATION

Corresponding Author

Perumal Ramamurthy − *National Centre for Ultrafast Processes, University of Madras, Chennai 600113, India; Department of Chemistry, Indian Institute of Technology-Madras, Chennai 600036, India;* orcid.org/0000-0003-2565-6236; Email: prm60@hotmail.com

Authors

Muthukumaran Nirmala − *National Centre for Ultrafast Processes, University of Madras, Chennai 600113, India*

Ramanan Vadivel − *Forensic Sciences Department, Government of Tamil Nadu, Chennai 600004, India;* orcid.org/0000-0003-1794-3518

Selvaraju Chellappan − *National Centre for Ultrafast Processes, University of Madras, Chennai 600113, India;* orcid.org/0000-0002-3625-4243

Jan Grzegorz Malecki − *Department of Crystallography, Silesian University, Katowice 40-006, Poland*

Complete contact information is available at: https://pubs.acs.org/10.1021/acsomega.1c00679

Notes

The authors declare no competing financial interest.

ACKNOWLEDGMENTS

The authors M.N. and P.R. thank D. S. Kothari postdoctoral fellowship (DSKPDF-fellow no. CH/18-19/0177) scheme for financial support in the form of fellowship. V.R. thanks the Director, M. Srinivasan, the Deputy Director, A. Visalakshi, and the Assistant Director, K. Manivannan, Forensic Sciences Department, Government of Tamil Nadu, Chennai for their support.

REFERENCES

(1) Hopkinson, M. N.; Richter, C.; Schedler, M.; Glorius, F. An overview of N-heterocyclic carbenes. *Nature* **2014**, *510*, 485−496.

(2) Hahn, F. E.; Jahnke, M. C. Heterocyclic carbenes: synthesis and coordination chemistry. *Angew. Chem., Int. Ed.* **2008**, *47*, 3122−3172.

(3) Vasylevskyi, S. I.; Regeta, K.; Ruggi, A.; Petoud, S.; Piguet, C.; Fromm, K. M. cis- and trans-9,10-di(1H-imidazole-1-yl)-anthracene based coordination polymers of ZnII and CdII: synthesis, crystal structures and luminescence properties. *Dalton Trans.* **2018**, *47*, 596−607.

(4) Sakai, H.; Kubota, T.; Yuasa, J.; Araki, Y.; Sakanoue, T.; Takenobu, T.; Wada, T.; Kawai, T.; Hasobe, T. Protonation-induced red-coloured circularly polarized luminescence of [5]carbohelicene fused by benzimidazole. *Org. Biomol. Chem.* **2016**, *14*, 6738−6743.

(5) Liu, L.; Wang, S.-M.; Han, Z.-B.; Ding, M.; Yuan, D.-Q.; Jiang, H.-L. Exceptionally Robust In-Based Metal−Organic Framework for Highly Efficient Carbon Dioxide Capture and Conversion. *Inorg. Chem.* **2016**, *55*, 3558−3565.

(6) Zhan, S.-J.; Sun, Y.; Li, S.-P.; Tang, G.-M.; Wang, Y.-T.; Cui, Y.-Z. Syntheses, crystal structures and luminescent properties of three metal coordination polymers based on aromatic carboxylic acids and 2-(pyridine-4-yl)-(1H)-benzoimidazole. *Polyhedron* **2017**, *121*, 252−263.

(7) Islamoglu, T.; Behera, S.; Kahveci, Z.; Tessema, T.-D.; Jena, P.; El-Kaderi, H. M. Facile Approach to Preparing Microporous Organic Polymers through Benzoin Condensation. *ACS Appl. Mater. Interfaces* **2016**, *8*, 14648−14655.

(8) Bansal, Y.; Silakari, O. The therapeutic journey of benzimidazoles: A review. *Bioorg. Med. Chem.* **2012**, *20*, 6208−6236.

(9) Peng, X.-M.; Cai, G.-X.; Zhou, C.-H. Recent developments in azole compounds as antibacterial and antifungal agents. *Curr. Top. Med. Chem.* **2013**, *13*, 1963−2010.

(10) Alfonso, M.; Tárraga, A.; Molina, P. Pyrrole, imidazole, and triazole derivatives as ion-pair recognition receptors. *Tetrahedron Lett.* **2016**, *57*, 3053−3059.

(11) Pashaei, B.; Shahroosvand, H.; Graetzel, M.; Nazeeruddin, M. K. Influence of Ancillary Ligands in Dye-Sensitized Solar Cells. *Chem. Rev.* **2016**, *116*, 9485−9564.

(12) Herrmann, W. A.; Köcher, C. N-Heterocyclic Carbenes. *Angew. Chem., Int. Ed. Engl.* **1997**, *36*, 2162−2187.

(13) Arduengo, A. J., III Looking for Stable Carbenes: The Difficulty in Starting Anew. *Acc. Chem. Res.* **1999**, *32*, 913−921.

(14) Bourissou, D.; Guerret, O.; Gabbaï, F. P.; Bertrand, G. Stable Carbenes. *Chem. Rev.* **2000**, *100*, 39−92.

(15) Arduengo, A. J., III; Harlow, R. L.; Kline, M. A stable crystalline carbene. *J. Am. Chem. Soc.* **1991**, *113*, 361−363.

(16) Arduengo, A. J., III; Davidson, F.; Dias, H. V. R.; Goerlich, J. R.; Khasnis, D.; Marshall, W. J.; Prakasha, T. K. An Air Stable Carbene and Mixed Carbene "Dimers". *J. Am. Chem. Soc.* **1997**, *119*, 12742−12749.

(17) Hemmert, C.; Gornitzka, H. Luminescent bioactive NHC−metal complexes to bring light into cells. *Dalton Trans.* **2016**, *45*, 440−447.

(18) Gonell, S.; Poyatos, M.; Peris, E. Pyrene-Based Bisazolium Salts: From Luminescence Properties to Janus-Type Bis-N-Heterocyclic Carbenes. *Chem.—Eur J.* **2014**, *20*, 9716−9724.

(19) Schuster, O.; Mercs, L.; Albrecht, M. The Potential of N-Heterocyclic Carbene Complexes as Components for Electronically Active Materials. *Chimia* **2010**, *64*, 184−187.

(20) Mercs, L.; Albrecht, M. Beyond catalysis: N-heterocyclic carbene complexes as components for medicinal, luminescent, and functional materials applications. *Chem. Soc. Rev.* **2010**, *39*, 1903−1912.

(21) Prabusankar, G.; Muthukumaran, N.; Vaddamanu, M.; Raju, G.; Velappan, K.; Sathyanarayana, A.; Masaya, Y.; Sugiyama, S.; Hisano, K.; Tsutsumi, O. Blue-emitting acridine-tagged silver(I)-bis-Nheterocyclic Carbene. *RSC Adv.* **2019**, *9*, 7543−7550.

(22) Visbal, R.; Ospino, I.; López-de-Luzuriaga, J. M.; Laguna, A.; Gimeno, M. C. N-Heterocyclic Carbene Ligands as Modulators of Luminescence in Three-Coordinate Gold(I) Complexes with Spectacular QuantumYields. *J. Am. Chem. Soc.* **2013**, *135*, 4712−4715.

(23) Gimeno, M. C.; Laguna, A.; Visbal, R. N-Heterocyclic Carbene Coinage Metal Complexes as Intense Blue-Green Emitters. *Organometallics* **2012**, *31*, 7146−7157.

(24) Citta, A.; Schuh, E.; Mohr, F.; Folda, A.; Massimino, M. L.; Bindoli, A.; Casini, A.; Rigobello, M. P. Fluorescent silver(I) and gold(I) N-heterocyclic carbene complexes with cytotoxic properties: mechanistic insights. *Metallomics* **2013**, *5*, 1006−1015.

(25) Bertrand, B.; de Almeida, A.; van der Burgt, E. P. M.; Picquet, M.; Citta, A.; Folda, A.; Rigobello, M. P.; Le Gendre, P.; Bodio, E.; Casini, A. New Gold(I) Organometallic Compounds with Biological Activity in Cancer Cells. *Eur. J. Inorg. Chem.* **2014**, *2014*, 4532−4536.

(26) Mercs, L.; Albrecht, M. Beyond catalysis: N-heterocyclic carbene complexes as components for medicinal, luminescent, and functional materials applications. *Chem. Soc. Rev.* **2010**, *39*, 1903−1912.

(27) Kido, J.; Kimura, M.; Nagai, K. Multilayer white light-Emitting Organic Electroluminescent Device. *Science* **1995**, *267*, 1332−1334.

(28) Dong, Y.; Xu, B.; Zhang, J.; Tan, X.; Wang, L.; Chen, J.; Lv, H.; Wen, S.; Li, B.; Ye, L.; Zou, B.; Tian, W. Piezochromic luminescence based on the molecular aggregation of 9,10-bis((E)-2-(pyrid-2-yl)vinyl)anthracene. *Angew. Chem., Int. Ed.* **2012**, *51*, 10782−10785.

(29) Sagara, Y.; Kato, T. Mechanically induced luminescence changes in molecular assemblies. *Nat. Chem.* **2009**, *1*, 605−610.

(30) Kobayashi, H.; Ogawa, M.; Alford, R.; Choyke, P. L.; Urano, Y. New Strategies for Fluorescent Probe Design in Medical Diagnostic Imaging. *Chem. Rev.* **2010**, *110*, 2620−2640.

(31) Oushiki, D.; Kojima, H.; Terai, T.; Arita, M.; Hanaoka, K.; Urano, Y.; Nagano, T. Development and Application of a Near-Infrared Fluorescence Probe for Oxidative Stress Based on Differential Reactivity of Linked Cyanine Dyes. *J. Am. Chem. Soc.* **2010**, *132*, 2795−2801.

(32) Zhao, Q.; Huang, C.; Li, F. Phosphorescent heavy-metal complexes for bioimaging. *Chem. Soc. Rev.* **2011**, *40*, 2508−2524.
(33) Eliseeva, S. V.; Bünzli, J.-C. G. Lanthanide luminescence for functional materials and bio-sciences. *Chem. Soc. Rev.* **2010**, *39*, 189−227.
(34) Li, Z.; Zhang, Y.; Jiang, S. Multicolor Core/Shell-Structured Upconversion Fluorescent Nanoparticles. *Adv. Mater.* **2008**, *20*, 4765−4769.
(35) Winnik, F. M. Photophysics of preassociated pyrenes in aqueous polymersolutions and in other organized media. *Chem. Rev.* **1993**, *93*, 587−614.
(36) Karuppannan, S.; Chambron, J.-C. Supramolecular chemical sensors based on pyrene monomer-excimer dual luminescence. *Chem.−Asian J.* **2011**, *6*, 964−984.
(37) Figueira-Duarte, T. M.; Müllen, K. Pyrene-based materials for organic electronics. *Chem. Rev.* **2011**, *111*, 7260−7314.
(38) Berlman, I. B.. *Handbook of Fluorescence Spectra of Aromatic Molecules*; Academic Press: New York, 1971.
(39) Oyamada, T.; Uchiuzou, H.; Akiyama, S.; Oku, Y.; Shimoji, N.; Matsushige, K.; Sasabe, H.; Adachi, C. Lateral organic light-emitting diode with field-effect transistor characteristics. *J. Appl. Phys.* **2005**, *98*, 074506−074512.
(40) Wang, Q.; Liu, H.; Lu, H.; Xu, Z.; Lai, G.; Li, Z.; Mack, J.; Shen, Z. Synthesis, characterization and solid-state emission properties of arylsilyl-substituted pyrene derivatives. *Dyes Pigm.* **2013**, *99*, 771−778.
(41) *Solid State Luminescence: Theory, materials and devices*; Kitai, A. H., Ed. ISBN 978-94-011-1522-3, Springer: Netherlands, 1993.
(42) Rahman, A. Z. M. S. *Solid State Luminescent Materials: Applications, Reference Module in Materials Science and Materials Engineering*; Elsevier publications: 2016.
(43) Wang, M.; Li, M.; Yu, A.; Zhu, Y.; Yang, M.; Mao, C. Fluorescent Nanomaterials for the Development of Latent Fingerprints in Forensic Sciences. *Adv. Funct. Mater.* **2017**, *27*, 1606243−1606258.
(44) Karami, K.; Ramezanpour, A.; Zakariazadeh, M.; Shahpiri, A.; Kharaziha, M.; Kazeminasab, A. Luminescent Palladacycles Containing a Pyrene, Chromophor; Synthesis, Biological and Computational, Studies of the Interaction with DNA and BSA. *ChemistrySelect* **2019**, *4*, 5126−5137.
(45) Ibrahim, H.; Koorbanally, N. A.; Ramjugernath, D.; Bala, M. D.; Nyamori, V. O. Synthesis and Characterization of Imidazolium Salts Bearing Fluorinated Anions. *Z. Anorg. Allg. Chem.* **2012**, *638*, 2304−2309.
(46) Freire, M. G.; Neves, C. M. S. S.; Marrucho, I. M.; Coutinho, J. A. P.; Fernandes, A. M. Hydrolysis of Tetrafluoroborate and Hexafluorophosphate Counter Ions in Imidazolium-Based Ionic Liquids. *J. Phys. Chem. A* **2010**, *114*, 3744−3749.
(47) de Robillard, G.; Makni, O.; Cattey, H.; Andrieu, J.; Devillers, C. H. Towards sustainable synthesis of pyren-1-yl azoliums via electrochemical oxidative C−N coupling. *Green Chem.* **2015**, *17*, 4669−4679.
(48) McGlynn, S. P.; Azumi, T.; Kinoshita, M.. *Molecular Spectroscopy of the Triplet State*; Prentice-Hall: Englewood Cliffs, NJ, 1969.
(49) Martinho, J. M. G. Heavy-Atom Quenching of Monomer and Excimer Pyrene Fluorescence. *J. Phys. Chem.* **1989**, *93*, 6687−6692.
(50) Kalyanasundaram, K.; Thomas, J. K. Environmental effects on vibronic band intensities in pyrene monomer fluorescence and their application in studies of micellar systems. *J. Am. Chem. Soc.* **1977**, *99*, 2039−2044.
(51) Birks, J. B. *Rep. Prog. Phys.* **1975**, *38*, 903−974.
(52) Winnik, F. M. Photophysics of Preassociated Pyrenes in Aqueous Polymer Solutions and in Other Organized Media. *Chem. Rev.* **1993**, *93*, 587−614.
(53) Ramamurthy, K.; Ponnusamy, K.; Chellappan, S. Excitation-resolved area-normalized emission spectroscopy: a rapid and simple steady-state technique for the analysis of heterogeneous fluorescence. *RSC Adv.* **2020**, *10*, 998−1006.
(54) Vadivel, R.; Nirmala, M. Visualization of Latent Fingerprints using Neutral Alumina as an Inexpensive Fingerprint Developing Powder. *Int. J. Forensic Sci. Pathol.* **2020**, *3*, 5−10.
(55) Maltoni, D.; Maio, D.; Jain, A. K.; Prabhakar, S. *Handbook of fingerprint recognition*; 2nd ed.; Springer-Verlag: New York, 2009.
(56) Perrin, D. D.; Armarego, W. L. F. *Purification of Laboratory Chemicals*; 3rded.; Pergamon Press: London, 1988.
(57) Sheldrick, G. M. A short history of SHELX. *Acta Crystallogr., Sect. A: Found. Crystallogr.* **2008**, *64*, 112−122.

https://doi.org/10.1021/acsomega.1c00679
ACS Omega 2021, 6, 10318−10332